Two-photon microwave transitions and strong-field effects in a room-temperature Rydberg-atom gas

D. A. Anderson,* A. Schwarzkopf, S. A. Miller, N. Thaicharoen, and G. Raithel
Department of Physics, University of Michigan, Ann Arbor, Michigan 48109, USA

J. A. Gordon and C. L. Holloway
National Institute for Standards and Technology, U.S. Department of Commerce, Boulder, Colorado 80305, USA
(Received 10 August 2014; published 29 October 2014)

We investigate two-photon Autler-Townes splitting and strong-field effects of ^{85}Rb Rydberg atoms in a room-temperature vapor cell. To observe the level structure we employ electromagnetically induced transparency. We first study the two-photon $62S_{1/2}$-$63S_{1/2}$ microwave transition using an electric-field reference measurement obtained with the one-photon $62S_{1/2}$-$62P_{3/2}$ transition. We then study the $61D_{5/2}$-$62D_{5/2}$ transition where the microwave electric-field range is extended up to $\sim$40 V/m. A Floquet analysis is used to model field-induced level shifts and state-mixing effects present in the strongly driven quantum systems under consideration. Calculations are found to be in good agreement with experimental observations.

DOI: 10.1103/PhysRevA.90.043419 PACS number(s): 32.80.Rm, 42.50.Gy, 32.30.Bv, 32.80.Ee

I. INTRODUCTION

Studies of interactions between atoms in highly excited Rydberg states and radiation fields have a rich history [1,2] and continue to provide a fertile ground for new physics. Strong Rydberg-field and Rydberg-Rydberg interactions have recently given rise to a range of studies in quantum optics and quantum many-body physics. These include the development of efficient single-photon sources [3,4] using electromagnetically induced transparency with Rydberg atoms (Rydberg-EIT) [5–7] and all-optical quantum processing by manipulation of Rydberg polariton states [8] using microwaves [9]. Efforts in establishing atomic standards [10] for field quantities have also benefited from the high sensitivity of Rydberg atoms. Room-temperature microwave electrometry by Autler-Townes (AT) splitting of Rydberg-EIT resonances [11] has recently been demonstrated as a viable high-precision technique [12] suitable for broadband measurements of radiation fields [13]. This technique has also been used for measurements of microwave polarizations [14], millimeter-wave detection [15], subwavelength imaging, and field mapping [16,17].

In this paper we study two-photon transitions and strong-field effects in room-temperature ^{85}Rb Rydberg atoms via Rydberg-EIT-AT. We consider two cases. In the first case, we probe a two-photon $nS_{1/2} \rightarrow (n+1)S_{1/2}$ transition. This transition has a dominant near-resonant intermediate state $nP_{3/2}$, which leads to large two-photon Rabi frequencies and considerable state mixing already at small microwave electric-field strengths. Generally, at low fields the system can be modeled quite well by perturbation theory. We compare the perturbative model with a (nonperturbative) Floquet analysis to account for higher-order field-induced mixing. In the second case, we study a two-photon $nD_{5/2} \rightarrow (n+1)D_{5/2}$ transition. This transition has no near-resonant intermediate state and requires higher electric fields to cause AT splittings. Here, we use a Floquet analysis to accurately model the system.

II. EXPERIMENTAL SETUP

Our setup, shown in Fig. 1(a), includes a probe laser beam at a wavelength of $\lambda_p \simeq 780$ nm and a coupling laser beam at a wavelength of $\lambda_c \simeq 480$ nm. The beams are overlapped and counterpropagating through a room-temperature cylindrical rubidium vapor cell that has a length of 75 mm and a diameter of 25 mm. The probe beam has a power of 200 nW and is focused to 80 μm full width at half maximum (FWHM); the coupling beam has a power of 24 mW and is focused to 100 μm FWHM. Each laser beam is linearly polarized along z and has a linewidth of $\sim$1 MHz. In each of our experiments, we use a four-level Rydberg-EIT-AT scheme, such as the one shown in Fig. 1(b). The probe laser frequency is scanned linearly across the $|5S_{1/2}\rangle \rightarrow |5P_{3/2}, F=4\rangle$ transition at a 1-Hz repetition rate, while the coupling laser frequency is fixed near a $|5P_{3/2}, F=4\rangle \rightarrow |\text{Rydberg}\rangle$ transition. The coupling laser intensity is modulated with a 10-kHz square wave by an acousto-optic modulator, and the transmitted probe power is measured by a photodiode. The photodiode signal is processed with a lock-in amplifier, the output of which is recorded by a digital oscilloscope. Microwaves in the K_u band (12–18 GHz) are produced by a signal generator and are emitted from a horn oriented as shown in Fig. 1(a). For most cases, the horn is placed 33 cm from the location of the laser beams. For the $nD_{5/2} \rightarrow (n+1)D_{5/2}$ case, the horn is placed up against the vapor cell to achieve higher power. The microwaves are linearly polarized along z (parallel to the optical beam polarizations). The experimental region is surrounded by microwave-absorbing material to avoid unwanted reflections.

Rydberg-EIT resonances are absorption minima of a weak probe beam, induced by the application of a strong coupling field between the upper probe level and a Rydberg state. We note that Rydberg-EIT differs from the traditional definition of EIT in that traditional EIT is defined for a Λ system in which two lower metastable levels are coupled to a common upper level that decays into each of the lower levels. In contrast, in our Rydberg-EIT system we are dealing with a cascade level scheme in which the uppermost (Rydberg) level decays slowly into other levels, including the intermediate $5P_{3/2}$ level (which, in turn, decays back to the ground state $5S_{1/2}$). The net result

*anderda@umich.edu

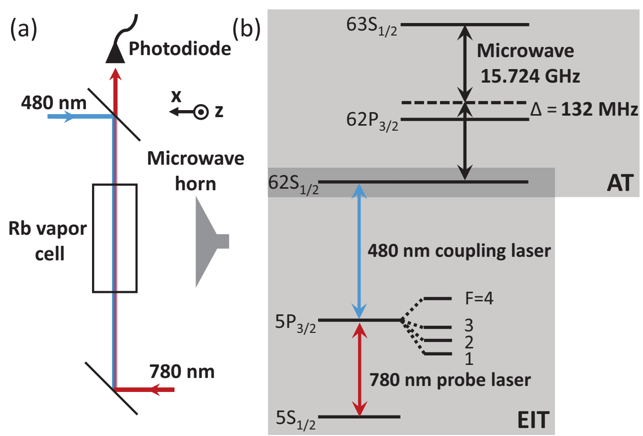

FIG. 1. (Color online) (a) Experimental setup (not to scale). (b) Energy-level diagram for the four-level cascade configuration and transitions used in the two-photon ^{85}Rb $62S_{1/2} - 63S_{1/2}$ Rydberg-EIT-AT measurement.

is that steady-state absorption of both fields is exactly zero in traditional EIT, whereas there is always a weak residual steady-state absorption of both fields in Rydberg-EIT. This reflects the fact that in Rydberg-EIT there is no perfectly dark state [6]. Despite these differences between traditional EIT and Rydberg-EIT, there are strong commonalities in the absorption and dispersion behavior of the probe field.

A Rydberg-EIT spectrum for the $|62S_{1/2}\rangle$ Rydberg state without the application of microwaves is shown in the top curve of Fig. 2(a). The plot is centered on the EIT signal of the $|5P_{3/2}, F = 4\rangle$ hyperfine state. This EIT resonance has a linewidth of $2\pi \times (3.4 \pm 0.3)$ MHz, which is larger than the $\approx 2\pi \times 1$ MHz single-atom EIT linewidth given by $\gamma_{\rm EIT} = \Omega_c^2/\gamma$ [18], where Ω_c is the Rabi frequency of the coupling field and γ is the $5P_{3/2}$ state linewidth. The observed EIT linewidth is likely increased by laser linewidths and transit-time broadening [18,19], however in our experiment the broadening is mostly due to the drift of the probe laser frequency over the course of one data-averaging sequence. The smaller feature at ≈ -48 MHz is an EIT signal of the $|5P_{3/2}, F = 3\rangle$ hyperfine state.

The application of a microwave field that couples the laser-excited Rydberg level to a second Rydberg level results in AT splitting of the EIT resonance. The frequency separation of the two EIT-AT peaks provides a measure of the microwave electric-field strength. In the experimental spectra, the measured frequency separations between EIT lines are altered due to different Doppler shifts of the coupling and probe beam frequencies. The frequency separations of the EIT resonances due to the $5P_{3/2}$ hyperfine structure are changed by a factor of $1 - \lambda_c/\lambda_p$, and those of the Rydberg levels (e.g., the microwave-induced AT splittings) are changed by a factor of λ_c/λ_p from their Doppler-free values [7].

III. ONE-PHOTON $62S_{1/2}$-$62P_{3/2}$

The sensitivity of Rydberg-EIT to radiation fields is due to the large electric dipole matrix elements of Rydberg-Rydberg transitions, which are typically $d \gtrsim 10^3 e a_0$, where e and a_0 are the elementary charge and the Bohr radius, respectively. This results in a strong atomic response to radiation fields at frequencies near an atomic transition; $\sim$8-μV/cm fields have previously been measured [12]. To obtain a field strength reference in the measurement volume, we first drive a one-photon dipole-allowed Rydberg-Rydberg transition. Figure 2(a) shows a series of Rydberg-EIT spectra for the $62S_{1/2}$-$62P_{3/2}$ Rydberg transition driven with the microwave source set at $\nu_{\rm MW} = 15.590\,464$ GHz. (This is within 1 MHz of the $62S_{1/2}$-$62P_{3/2}$ transition frequency calculated using

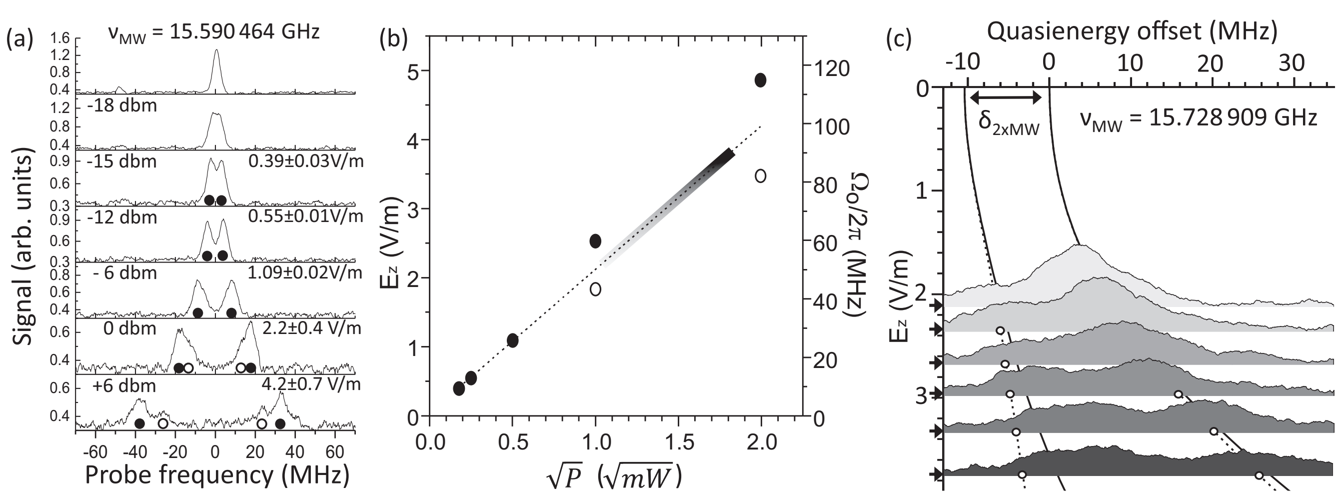

FIG. 2. (a) Rydberg-EIT-AT spectra for the one-photon $62S_{1/2}$-$62P_{3/2}$ Rydberg transition for increasing microwave power (top to bottom). (b) Measured Rabi frequency and electric-field strength for the inner (white) and outer (black) maxima in (a) are plotted versus the square root of applied microwave power. Line centers are determined by Gaussian fits to the peaks. Uncertainty bars, given by the fit error, are smaller than the data points. The dashed line is a linear fit to the average measured field strength. The shaded region indicates the microwave field range for the $62S_{1/2}$-$63S_{1/2}$ measurement in (c). (c) $62S_{1/2}$-$63S_{1/2}$ spectra at average field strengths indicated by the arrows. State energies obtained from second-order perturbation theory are plotted as a function of average microwave field (solid lines); also plotted are quasienergies from a Floquet analysis for the $62S_{1/2}$ and $63S_{1/2}$ state pair (dashed lines). All spectra in (a) and (c) are averages of 12 and 15 traces, respectively.

quantum defects from Ref. [2].) As the microwave power is increased, there is an increased splitting of the EIT resonance into two symmetric EIT-AT peaks. Generally, for both single and multiphoton transitions, the observed frequency splittings correspond to $\lambda_c/\lambda_p \times \tilde{\Omega}$, where $\tilde{\Omega} = \sqrt{\delta^2 + \Omega_0^2}$ is the effective Rabi frequency. Here, δ is the detuning of the microwave frequency from the Rydberg-Rydberg transition, and Ω_0 is the (on-resonant) Rabi frequency of the transition. For the data in Fig. 2(a), $\delta \approx 0$, and from the splitting of the EIT-AT peaks at each microwave power we obtain Ω_0 for the $62S_{1/2}$-$62P_{3/2}$ transition. The z-polarized microwave field strength E_z is then determined from $E_z = \Omega_0 \hbar / d_z$ using the measured Ω_0 and the calculated electric dipole matrix element $d_z = 1854 e a_0$ for the $|62S_{1/2}, m_j = 1/2\rangle - |62P_{3/2}, m_j = 1/2\rangle$ transition.

In principle, the width of the individual AT line profiles is given by the decay rates of the two coupled states [20]. Here, since none of the Rydberg states involved has a substantial decay rate, we assume the AT linewidths are primarily determined by inhomogeneous line broadening. Specifically, as the microwave field is increased, the EIT-AT peaks become broadened due to inhomogeneity of the electric field inside the vapor cell. Atoms located at different positions within the path of the probe beam sample different field strengths. At the highest microwave powers in Fig. 2(a), each of the EIT-AT peaks exhibits two separated maxima as indicated by the black and white circles. We attribute this to local extrema in the electric-field distribution in the vapor cell (see, for example, Ref. [17]). The average field strengths are indicated in Fig. 2(a). In Fig. 2(b) we show a plot of the Rabi frequencies measured in Fig. 2(a) and the corresponding field strengths as a function of the square root of the microwave power. The black circles correspond to the separation of the outer maxima, and the white circles correspond to that of the inner maxima. Based on the data in Figs. 2(a) and 2(b), the uncertainty in the field strength is estimated to be $\pm 15\%$. The dashed line in Fig. 2(b) is a fit to the average measured field, showing the expected linear dependence of the single-photon transition Rabi frequency on the microwave field.

We note that field-induced state mixing must generally be considered in the interpretation of Figs. 2(a) and 2(b). Floquet calculations (discussed in detail below) show that over the measured field range in Fig. 2(a) the electric dipole moment of the $62S_{1/2}$-$62P_{3/2}$ transition drops by $\sim 6\%$ from its zero-field value of $d_z = 1854 e a_0$. Accounting for this would result in a slight nonlinear correction to the electric-field axis in Fig. 2(b). In our present paper, this correction is less than the electric-field uncertainty and is therefore ignored.

IV. TWO-PHOTON $62S_{1/2}$-$63S_{1/2}$

In our multiphoton work, we first study the $62S_{1/2}$-$63S_{1/2}$ two-photon transition. We use microwave field strengths that are within the measurement range in Figs. 2(a) and 2(b). Considering only the dominant $62P_{3/2}$ intermediate state as shown in Fig. 1(b), the two-photon Rabi frequency can be expressed as $\Omega_{2\times\mathrm{MW}} = \Omega_1 \Omega_2 / (2\Delta)$, where Ω_1 and Ω_2 are the single photon $62S_{1/2}$-$62P_{3/2}$ and $62P_{3/2}$-$63S_{1/2}$ Rabi frequencies, respectively, and Δ is the detuning of the microwave frequency from the $62P_{3/2}$ intermediate state. For the $62S_{1/2}$-$63S_{1/2}$ transition, $\Omega_1 \approx \Omega_2$ to within 3%. Furthermore, since $\Delta > \Omega_1$, we expect $\Omega_{2\times\mathrm{MW}}$ to be smaller than Ω_1 by a factor of $\approx \Omega_1/(2\Delta)$. For the levels shown in Fig. 1(b) and the full electric-field range of 0.4–4.2 V/m covered in Figs. 2(a) and 2(b), this corresponds to Rabi-frequency ratios of $\Omega_{2\times\mathrm{MW}}/\Omega_1 \ \sim 1/30$ to 1/3, respectively.

We drive the $62S_{1/2}$-$63S_{1/2}$ two-photon transition shown in Fig. 1(b) at $\nu_{\mathrm{MW}} = 15.728\,909$ GHz for microwave field strengths over the range indicated by the gray-shaded region in Fig. 2(b). This two-photon microwave frequency ($2 \times \nu_{\mathrm{MW}}$) is blue detuned from the $62S_{1/2}$-$63S_{1/2}$ transition by $\delta_{2\times\mathrm{MW}}/2\pi = 10$ MHz. The $62S_{1/2}$-$63S_{1/2}$ two-photon EIT-AT spectra are shown in Fig. 2(c) where the frequency axes of the experimental spectra have been scaled by λ_p/λ_c so that the AT splittings correspond directly to the effective two-photon Rabi frequency $\tilde{\Omega}_{2\times\mathrm{MW}}$. It is evident that $\tilde{\Omega}_{2\times\mathrm{MW}}$ is considerably smaller than Ω_1. Taking into account the nonzero $\delta_{2\times\mathrm{MW}}$, for the electric-field range from 2.12 to 3.74 V/m we measure Rabi-frequency ratios $\tilde{\Omega}_{2\times\mathrm{MW}}/\Omega_1$ of $\sim 1/5$ to 1/3, respectively. These fall within the expected range. Due to the quadratic field dependence of the two-photon Rabi frequency, the $\pm 15\%$ uncertainty in the electric field leads to an inhomogeneous broadening of the two-photon $62S_{1/2}$-$63S_{1/2}$ AT lines that is $\approx \pm 30\%$ of $\Omega_{2\times\mathrm{MW}}$. This is seen in the $62S_{1/2}$-$63S_{1/2}$ spectra in Fig. 2(c) where the broadening approaches the effective two-photon Rabi frequency. The large broadening seems to obscure any AT-splitting substructure caused by field extrema as seen in the $62S_{1/2}$-$62P_{3/2}$ spectra in Fig. 2(a).

To model the energy-level shifts observed in Fig. 2(c), we first use a perturbative treatment considering off-resonant transitions through the intermediate $62P_{1/2}$ and $62P_{3/2}$ levels. The dominant coupling is through the $62P_{3/2}$ level; the two-photon Rabi frequency through this intermediate level is about a factor of 6 larger than the one through the $62P_{1/2}$ level. This difference is in part due to the intermediate-state detunings, which are ~ 150 MHz for $62P_{3/2}$ and ~ 500 MHz for $62P_{1/2}$. In the perturbative model we first calculate the ac Stark shifts of the $62S_{1/2}$, $62P_{1/2}$, $62P_{3/2}$, and $63S_{1/2}$ states using second-order perturbation theory (see, for example, Ref. [21]). The $62S_{1/2}$ and $63S_{1/2}$ energies shift at about $+1.34$ and $+1.40$ MHz $(\mathrm{V/m})^{-2}$, respectively. This results in differential shifts of < 1 MHz in the experimental electric-field range, and therefore $\delta_{2\times\mathrm{MW}}$ does not noticeably change as a function of electric field. The intermediate $62P_{3/2}$ energy shifts at about -2.09 MHz $(\mathrm{V/m})^{-2}$, whereas the $62P_{1/2}$ energy does not shift significantly. Over the field range in Fig. 2(c), the $62P_{3/2}$ level shifts by an absolute amount of ≈ -9 to -29 MHz. Taking into account both $62S_{1/2}$ and $62P_{3/2}$ level shifts, the detuning Δ increases by about 25% over the same range. (The corresponding change in Δ for the further-off-resonant $62P_{1/2}$ level is insignificant.) The AT pair energies are then calculated by diagonalizing a 2×2 Hamiltonian with the $62S_{1/2}$ and $63S_{1/2}$ dressed energy-level shifts on the diagonals and the sum of the two-photon couplings through the $62P_{3/2}$ and $62P_{1/2}$ levels on the off-diagonals (where the field dependence of the Δ values is taken into account). The resulting energies are plotted as solid lines in Fig. 2(c). The residual energy splitting at zero field corresponds to $\delta_{2\times\mathrm{MW}}$. The ac Stark shifts and two-photon couplings in the

Hamiltonian are proportional to $|E|^2$ (with small deviations in the couplings due to the field dependence of Δ). Hence, for the case of a resonant two-photon $62S_{1/2}$-$63S_{1/2}$ interaction ($\delta_{2\times\mathrm{MW}} = 0$), the eigenvalues and AT splittings would scale approximately as $|E|^2$. For a nonzero detuning, the energy-level spectrum exhibits a more complex behavior. In the limit $\delta_{2\times\mathrm{MW}} > \Omega_{2\times\mathrm{MW}}$, the AT levels have a near-constant energy splitting of $\hbar \times \delta_{2\times\mathrm{MW}}$. At large field strengths, when $\Omega_{2\times\mathrm{MW}} > \delta_{2\times\mathrm{MW}}$, the splitting approaches the $|E|^2$ scaling of the $\delta_{2\times\mathrm{MW}} = 0$ case. Our experiment is in a regime where $\delta_{2\times\mathrm{MW}} \approx \Omega_{2\times\mathrm{MW}}$. Here, the splitting does not exhibit a clear scaling behavior.

To investigate the influence of higher-order state mixing, we perform a Floquet analysis, which accounts for the effect of the microwave field in an exact nonperturbative manner [22]. The dashed lines in Fig. 2(c) are the calculated Floquet quasienergies of the $62S_{1/2}$ and $63S_{1/2}$ state pair as a function of average field strength for the 15.728 909-GHz microwaves. The quasienergies agree very well with the level shifts and AT splitting obtained using perturbation theory for field strengths up to 2 V/m. Beyond this field strength, in the Floquet calculation, the lower AT state becomes increasingly redshifted relative to that of the perturbative calculation; the difference reaches about 5 MHz at $E_z = 4$ V/m. This difference is due to higher-order couplings not accounted for in the perturbative calculation. Compared to both calculations, at larger electric-field strengths, the experimental spectra appear to shift to higher energies by a few megahertz. This is likely due to a drift of the coupling laser frequency over the entire measurement duration in Fig. 2(c). There is also a slight mismatch between experimental and calculated AT splittings. This may be explained by the uncertainty in the electric-field distribution.

The amount of $62S_{1/2}$ and $63S_{1/2}$ state character in the AT states depends on both the microwave field strength and the frequency detuning from the two-photon resonance. This effect is evident in Fig. 2(c) where the ratio of the EIT-AT peak areas changes as a function of the applied field strength for the given nonzero $\delta_{2\times\mathrm{MW}}$. At the smallest field, we preferentially excite the upper EIT-AT state, which is predominantly of $62S_{1/2}$ character. At higher microwave fields the $62S_{1/2}$ and $63S_{1/2}$ states are more strongly mixed, and the $62S_{1/2}$ character becomes evenly distributed between the two EIT-AT states. The Floquet analysis shows that for the data in Fig. 2(c) the signal-strength ratio of the lower and upper EIT-AT signals should vary from $\sim 1/6$ at the low-field end to $\sim 2/3$ at the high-field end. The analysis also shows considerable mixing of $\ell > 0$ states into the relevant Floquet levels [see Table I(a)]. This is primarily due to the small intermediate-state detuning Δ for the $62P_{3/2}$ level [see Fig. 1(b)], which results in substantial mixing of the $62P_{3/2}$ state with the $62S_{1/2}$ and $63S_{1/2}$ states at field strengths that are already quite low. As seen in Table I(a), the admixture percentages of the $\ell \neq 0$ states other than $62P$ are very small as one would expect for low field strengths.

V. TWO-PHOTON $61D_{5/2}$-$62D_{5/2}$

To extend the technique to higher-field strengths, we drive the two-photon $61D_{5/2}$-$62D_{5/2}$ transition at 15.116 35 GHz, which is within 0.5 MHz of the calculated transition frequency. The nearest dipole-allowed intermediate states for this transition are the $63P$ and $60F$ states from which the microwave frequency is detuned by ≈ -6 and $+5$ GHz, respectively. These detunings are about a factor of 40 larger than the intermediate-state detuning in the $62S_{1/2}$-$63S_{1/2}$ study, requiring significantly higher electric-field strengths to generate AT splittings. For this experiment we apply electric fields (intensities) that are $\sim 10\times$ ($\sim 100\times$) larger than those used in the $62S_{1/2}$-$63S_{1/2}$ study. Another important difference between the $62S_{1/2}$-$63S_{1/2}$ and the $61D_{5/2}$-$62D_{5/2}$ studies is that the latter involves levels with fine structure (FS). At high fields FS-changing microwave couplings into $D_{3/2}$ levels become important.

TABLE I. Admixture percentages into AT-split levels from states identified in the right column. Percentages given are averages over one microwave cycle. (a) For the $62S_{1/2}$-$63S_{1/2}$ transition and fields as in Fig. 2. (b) For the $61D_{5/2}$-$62D_{5/2}$ transition and fields as in Fig. 3. For the $62S_{1/2}$-$63S_{1/2}$ case we show total admixture percentages as well as admixture percentages excluding the mixing with the near-resonant intermediate $62P$ levels. For the $61D_{5/2}$-$62D_{5/2}$ case we show total admixture percentages as well as admixture percentages excluding fine-structure mixing.

		(a) $62S$-$63S$		
E (V/m)	$\lvert m_j\rvert = 1/2$			Character
2	2.75			$\ell \neq 0$
4	7.44			in $62S_{1/2}$ and $63S_{1/2}$
2	0.08			$\ell \neq 0$ excluding $62P$
4	0.29			in $62S_{1/2}$ and $63S_{1/2}$
		(b) $61D$-$62D$		
E (V/m)	$\lvert m_j\rvert = 1/2$	3/2	5/2	Character
13	0.37	0.36	0.12	$\ell \neq 2$, $61D_{3/2}$, $62D_{3/2}$
37	3.88	11.24	0.96	in $61D_{5/2}$ and $62D_{5/2}$
13	0.36	0.22	0.12	$\ell \neq 2$
37	2.90	1.75	0.96	in $61D_j$ and $62D_j$

To achieve higher microwave powers, the microwave horn is placed up against the vapor cell. We obtain two-photon EIT-AT spectra for a set of microwave source powers, incremented in steps of 1 dBm. An experimental density plot of these spectra is shown in Fig. 3, along with calculated Floquet quasienergies up to 87 V/m. The experimental spectra are aligned in frequency with the calculated Floquet quasienergies to account for 480-nm laser frequency drift; the experimental spectra (which have a fixed 1-dB spacing) are also adjusted along the logarithmic intensity scale by a common offset to match them with the calculation on an absolute microwave intensity scale. The agreement between experimental and calculated energies is quite good. Despite the fact that the $5S_{1/2}$ ground state only has a $|m_j| = 1/2$ component and all fields are z polarized, in the spectra we see states of both $|m_j| = 1/2$ and 3/2 character (short and long dashed lines, respectively). This is because most $|5P_{3/2}, F, m_F\rangle$ hyperfine levels contain multiple m_j components.

At the high-intensity end of the data in Fig. 3, the $|m_j| = 1/2$ and 3/2 components split into resolved nondegenerate AT pairs. The m_j degeneracy is lifted due to the $|m_j|$ dependence of the two-photon Rabi frequencies and ac Stark shifts. As

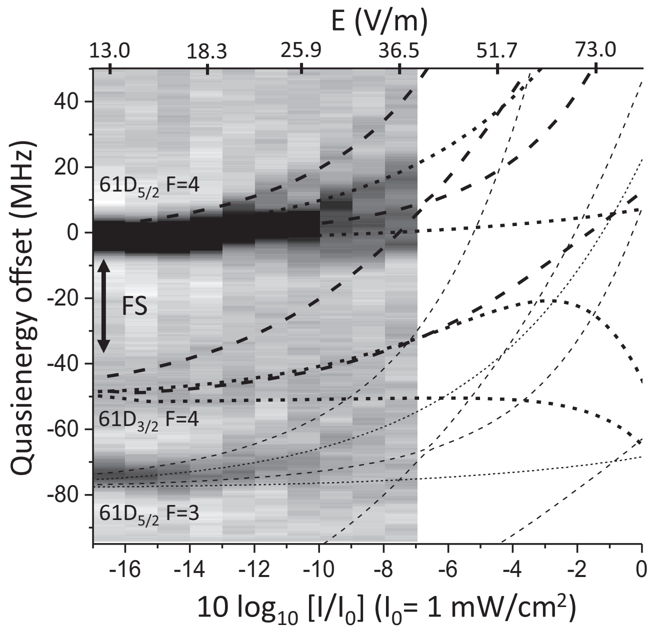

FIG. 3. Density plot of experimental two-photon $61D_{5/2}$-$62D_{5/2}$ EIT-AT spectra versus microwave intensity and field strength. The signal strength is represented on a linear gray scale from <0.26 (white) to >0.6 (black) in arbitrary units of the probe transmission. The fine-structure splitting at zero field of the $61D$ state is indicated on the plot (FS). Calculated Floquet quasienergies for states with significant $|m_j| = 1/2$ (short dashed lines) and $|m_j| = 3/2$ (long dashed lines) character are overlaid for the hyperfine EIT resonances $5P_{3/2}$ $F = 4$ (thick lines) and $F = 3$ (thin lines).

in the $62S_{1/2}$-$63S_{1/2}$ case [Fig. 2(c)], the couplings and ac Stark shifts for the $61D_{5/2}$-$62D_{5/2}$ case in the experimentally probed field range (Fig. 3) are approximately proportional to $|E|^2$. Allometric fits to most levels in Fig. 3 exhibit this quadratic scaling for fields $\lesssim 40$ V/m. For the lower components of the $|m_j| = 1/2$ AT pairs, the positive ac Stark shifts are nearly canceled by the AT level repulsions, leading to near-stationary level energies with allometric-fit exponents substantially different from 2.

The Floquet analysis reveals the mixing behavior of the AT-coupled levels. We distinguish between two types of mixing, namely, total mixing (including FS mixing) and ℓ mixing only (excluding FS mixing). Table I(b), upper rows, shows the total admixture percentages of the $61D_{5/2}$ and $62D_{5/2}$ AT pair (including $D_{3/2}$ states), for the lowest and highest field strengths probed in the experiment. Since the zero-field FS splittings are only ≈ 50 MHz, the admixing percentages are quite high due to substantial FS mixing (i.e., J-changing microwave couplings). In the bottom rows of Table I(b), we show ℓ-mixing percentages, i.e., admixtures from states with $\ell \neq 2$ into all $61D_j$ and $62D_j$ AT pairs with $J = 3/2$ or $5/2$. Despite the significantly larger electric-field strengths used in this $61D_{5/2}$-$62D_{5/2}$ study compared to the $62S_{1/2}$-$63S_{1/2}$ study, the mixing of $\ell \neq 2$ states into the $61D_j$ and $62D_j$ states in Fig. 3 is less than the mixing of $\ell \neq 0$ states into the $62S_{1/2}$ and $63S_{1/2}$ states in Fig. 2. This qualitatively different ℓ-mixing behavior is due to the larger detunings from dipole-allowed transitions into intermediate states in the $61D_{5/2}$-$62D_{5/2}$ case compared to the $62S_{1/2}$-$63S_{1/2}$ case.

Further analysis of the $|m_j| = 3/2$ and 1/2 Floquet states shows that they exhibit a transition from a FS-dominant into a microwave-coupling-dominant regime. In the latter, the microwave field is strong enough that it decouples electron and orbital spins (i.e., m_s and m_ℓ quantum numbers become separately conserved). This breakup of the FS occurs at lower fields for $|m_j| = 3/2$ (~ 40 V/m) than it does for $|m_j| = 1/2$ (~ 100 V/m). Table I(b) indicates that the FS mixing at 37 V/m is about three times as large for $|m_j| = 3/2$ than it is for $|m_j| = 1/2$. Inspection of Fig. 3 shows that the difference in FS breakup behavior follows from larger AT splittings (microwave couplings) and ac level shifts in the $|m_j| = 3/2$ levels compared to the $|m_j| = 1/2$ levels. It is also noted that at fields of $\gtrsim 50$ V/m deviations in the level shifts from an approximate E^2 scaling become substantial. In some cases there is even a change in sign of the dynamic electric dipole moment. This is related to the high density of states in the Floquet energy spectrum and the correspondingly large number of higher-order couplings which become effective at larger fields. An experimental study of the complex level structure in the FS breakup transition regime and beyond is an objective of future work.

VI. CONCLUSION

We have studied two-photon transitions in room-temperature ^{85}Rb atoms using Rydberg-EIT-AT for two cases. The first is an $nS \rightarrow (n+1)S$ transition with a single near-resonant intermediate nP state. The second is an $nD \rightarrow (n+1)D$ transition for higher electric-field strengths. Over a large range of field strengths, level shifts and field-induced state mixing effects were observed. In the first case, the Rydberg atom-field interactions were modeled using both perturbation theory and a Floquet treatment. To within the measurement uncertainty, both models reproduced the observed level shifts and AT splittings. In the second case, the system was modeled using the Floquet treatment, which reproduced the experiment rather well. Here, field-induced state-mixing percentages indicate a transition into a fine-structure mixing regime at the highest experimental field strengths. This paper exhibits the utility of room-temperature Rydberg-EIT for studies of strong Rydberg atom-field interactions. Our extension of Rydberg-EIT-AT to a strong-field regime also suggests the method may be well suited as an atom-based technique for precision field measurements of high-power radiation sources.

ACKNOWLEDGMENTS

We thank P. R. Berman for valuable discussions. This work was supported by the AFOSR and by DARPA's QuASAR program.

[1] *Rydberg States of Atoms and Molecules*, edited by R. F. Stebbings and F. B. Dunning (Cambridge University Press, Cambridge, UK, 1983).

[2] T. F. Gallagher, in *Rydberg Atoms*, edited by A. Dalgarno, P. L. Knight, F. H. Read, and R. N. Zare, Cambridge Monographs on Atomic, Molecular and Chemical Physics Vol. 3 (Cambridge University Press, Cambridge, UK, 1994).

[3] Y. O. Dudin and A. Kuzmich, Science **336**, 887 (2012).

[4] T. Peyronel, O. Firstenberg, Q.-Y. Liang, S. Hofferberth, A. V. Gorshkov, T. Pohl, M. D. Lukin, and V. Vuletic, Nature (London) **488**, 57 (2012).

[5] A. Krishna, K. Pandey, A. Wasan, and V. Natarajan, Europhys. Lett. **72**, 221 (2005).

[6] M. Fleischhauer, A. Imamoglu, and J. P. Marangos, Rev. Mod. Phys. **77**, 633 (2005).

[7] A. K. Mohapatra, T. R. Jackson, and C. S. Adams, Phys. Rev. Lett. **98**, 113003 (2007).

[8] M. D. Lukin, Rev. Mod. Phys. **75**, 457 (2003).

[9] D. Maxwell, D. J. Szwer, D. Paredes-Barato, H. Busche, J. D. Pritchard, A. Gauguet, K. J. Weatherill, M. P. A. Jones, and C. S. Adams, Phys. Rev. Lett. **110**, 103001 (2013).

[10] L. Essen and J. V. L. Parry, Nature (London) **176**, 280 (1955).

[11] B. K. Dutta and P. K. Mahapatra, Phys. Scr. **75**, 345 (2007).

[12] J. A. Sedlacek, A. Schwettmann, H. Kübler, R. Löw, T. Pfau, and J. P. Shaffer, Nat. Phys. **8**, 819 (2012).

[13] C. L. Holloway, J. A. Gordon, S. Jefferts, A. Schwarzkopf, D. A. Anderson, S. A. Miller, N. Thaicharoen, and G. Raithel, arXiv:1405.7066.

[14] J. A. Sedlacek, A. Schwettmann, H. Kübler, and J. P. Shaffer, Phys. Rev. Lett. **111**, 063001 (2013).

[15] J. A. Gordon, C. L. Holloway, A. Schwarzkopf, D. A. Anderson, S. Miller, N. Thaicharoen, and G. Raithel, Appl. Phys. Lett. **105**, 024104 (2014).

[16] H. Q. Fan, S. Kumar, R. Daschner, H. Kübler, and J. P. Shaffer, Opt. Lett. **39**, 3030 (2014).

[17] C. L. Holloway, J. A. Gordon, A. Schwarzkopf, D. A. Anderson, S. A. Miller, N. Thaicharoen, and G. Raithel, Appl. Phys. Lett. **104**, 244102 (2014).

[18] M. Erhard and H. Helm, Phys. Rev. A **63**, 043813 (2001).

[19] A. Sargsyan, D. Sarkisyan, U. Krohn, J. Keaveney, and C. Adams, Phys. Rev. A **82**, 045806 (2010).

[20] P. R. Berman and V. S. Malinovsky, *Principles of Laser Spectroscopy and Quantum Optics* (Princeton University Press, Princeton, NJ, USA, 2011).

[21] M. Haas, U. D. Jentschura, and C. H. Keitel, Am. J. Phys. **74**, 77 (2006).

[22] S. I. Chu, in *Advances in Chemical Physics*, edited by J. O. Hirschfelder, R. E. Wyatt, and R. D. Coalson (Wiley, New York, 1989), Vol. 73, pp. 739–799.